J MATER SCI **41** (2006) 3961–3972

Structure and mechanical properties of micro and macro balloons: An overview of test techniques

K. B. CARLISLE, K. K. CHAWLA
University of Alabama at Birmingham, Birmingham, AL 35294, USA

G. M. GLADYSZ
Los Alamos National Laboratory, Los Alamos, NM 87545, USA

M. KOOPMAN
University of Alabama at Birmingham, Birmingham, AL 35294, USA

Published online: 7 June 2006

A recently developed technique for obtaining uniaxial compression properties of individual microballoons by using a nanoindentation instrument equipped with a flat-ended tip of cylindrical or square cross-section will be described. A variety of useful parameters can be extracted from load vs. displacement curves such as: failure load, strain to failure, fracture energy, and a pseudo-stiffness or spring constant of each microballoon tested. The technique allows for a comparison of compression properties between individual microballoons of varying size or morphology. Other techniques for compression of both individual and large numbers of microballoons simultaneously, will be compared to this new test procedure. Two novel tensile test techniques will be reviewed. Additionally, the utility of complimentary test methods—including quantitative microscopy, SEM, interferometry, and nanoindentation—for characterizing the structure and properties of microballoons will be discussed.

1. Introduction

Originally, microballoons and macroballoons (note that microballoons will henceforth be abbreviated MBs, whereas macroballoons will not be abbreviated) were viewed as fillers, i.e. they provided increased specific properties while simultaneously reducing the amount of polymer used. Perusal of the product information sheets from current MB manufacturers still emphasizes this role. Increasingly, however, the reinforcement values of microballoons are also being realized. MBs are no longer relegated to the role of fillers but have become a second phase in polymer composites that can increase the material's properties significantly, especially compressive and impact strengths. Thus, a polymer part containing MBs can more appropriately be called a composite. Other uses for MBs are becoming more common as well. MBs can facilitate a sustained release of drugs contained in their hollows in the pharmaceutical industry, provide a mechanism for storage and release of adhesives in Post-It® notes, and release perfumes and moisturizers when broken in household products like detergents and skin care creams [1]. All of these applications are aided from a design standpoint by knowledge of the structure and properties of the MBs.

What has led to the proliferation of MB uses? Mostly, it is continued advances in production techniques, combined with an expanding range of materials from which microballoons may be manufactured. The original patents for producing polymer microballoons (PMBs), like those shown in Fig. 1, or glass microballoons (GMBs)—see Fig. 2—were merely the beginning of microballoon production. Techniques for producing MBs from other polymers, from the polyglycolic acid and polylactic acid used in drug encapsulation to hydrogels, have been developed. In producing such MBs, methods besides disk atomization of polymeric solutions containing blowing agents are being replaced by ultrasonic atomization for better particle size distribution control or even by emulsion techniques, where the microballoons are formed completely without the aid of blowing agents. Template methods for production have been considered. Additional advances have led the original MB technology to new

0022-2461
DOI: 10.1007/s10853-006-7571-y

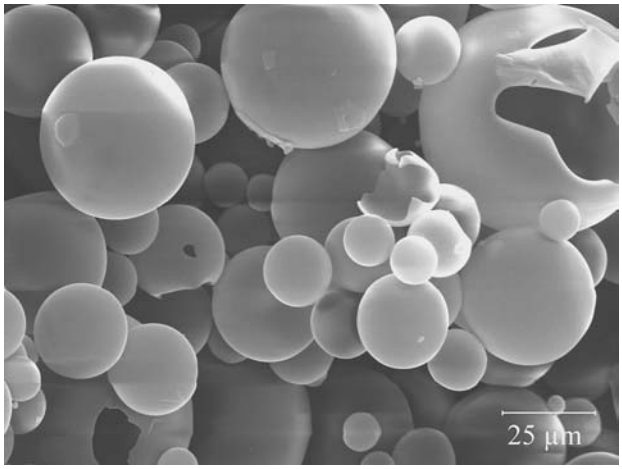

Figure 1 Phenolic microballoons, showing size range and many broken balloons. SEM.

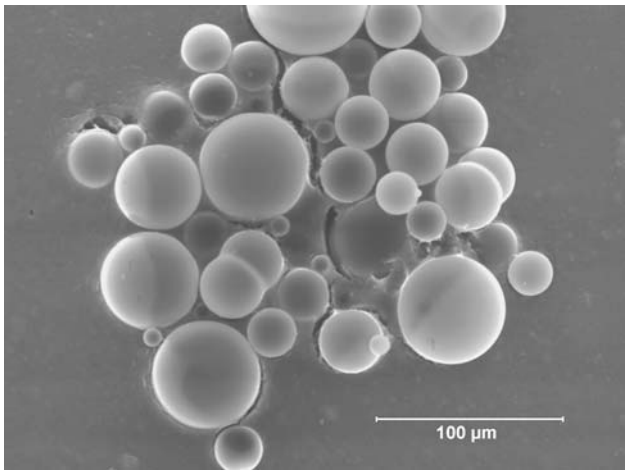

Figure 2 GMBs (3 M A16/500). Note the size range and regular morphology. SEM.

applications, such as the production or modification of glass microballoons for specialized applications and the polymeric microballoons that are being produced specifically for conversion via heat treatment to other materials, e.g., the carbon microballoons (CMBs) shown in Fig. 3 [2–4].

With this growth in the use of MBs and the technology associated with their production, so too must the ways of characterizing MBs grow. One of 3 M's early patents for producing glass microballoons specifically refers to a test technique using isostatic compression for measuring the strength of MBs. This technique would later become ASTM D 3602, which is still used for testing glass microballoons today, although the standard has been discontinued for unknown reasons. Other techniques that were used during the developmental phase of microballoons are in similar states, and are often the only tests routinely utilized to measure the mechanical characteristics of microballoons. However, many of today's applications differ

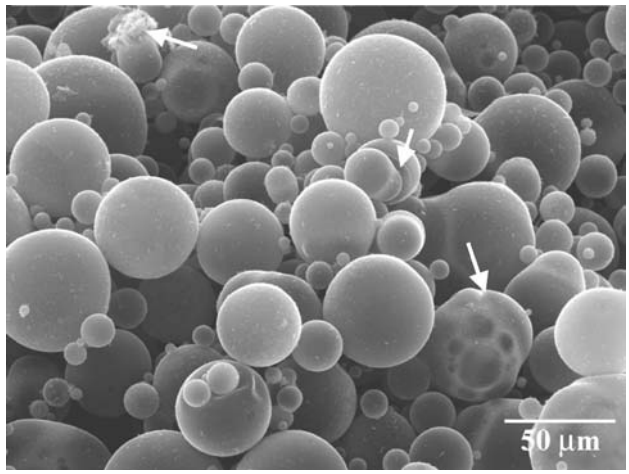

Figure 3 0.177 g/cm^3 tap density CMBs, showing general spherical morphology. Defects like multi-compartmented and broken MB also visible (arrows) SEM.

greatly from those initial applications, and thus require more mechanical property and structural information of the microballoons. This, then, becomes the primary goal of this review. We will strive to present the older established methods of microballoon characterization, the newer small scale test techniques that have been recently developed, and revisit some novel tests that never gained wide usage in microballoon testing. The goal is to describe the type and utility of the information obtained from each test technique, as well as to explore how a synergy of these methods may best provide an overall characterization of microballoons [5, 6].

2. Microscopic examination of microballoons

Scanning electron microscopy provides an invaluable tool for analyzing MB morphology. Provided that nonconducting samples are properly coated, almost any MB may be successfully imaged and useful data taken regarding its diameter as well as shape. Imaging of broken MBs can provide wall thickness data; wall thickness is often a property-controlling parameter of considerable interest. Fig. 4 provides some examples of CMB wall thickness measurements taken on broken MB via SEM [7, 8]. For accurate measurement of wall thickness, the broken wall must be perpendicular to the microscope axis, or the angle of inclination known, for correction.

Optical microscopy techniques complement SEM measurements, giving a cross sectional interior view of mounted and polished MBs. Optical images can be useful in analyzing the MBs' internal structure, wall thickness, and diameter. Conventional reflected light microscopy, as well as laser confocal microscopy and interference fringe microscopy, can be employed to advantage. The first method provides the traditional two dimensional images of a polished surface, as shown in Fig. 5. Care must

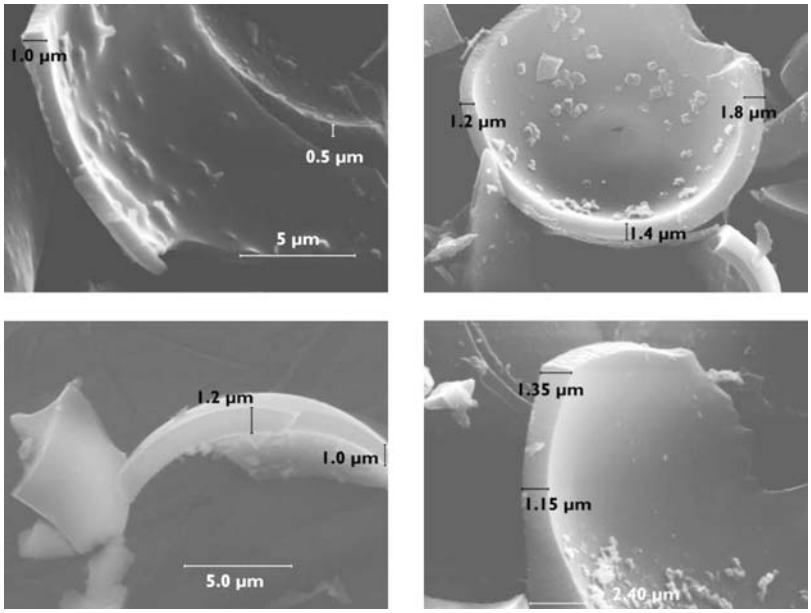

Figure 4 Wall thickness measurement of CMB fragments. Range of observed thickness in the figure is 0.5–2.4 μm. SEM. After refs. [7, 8].

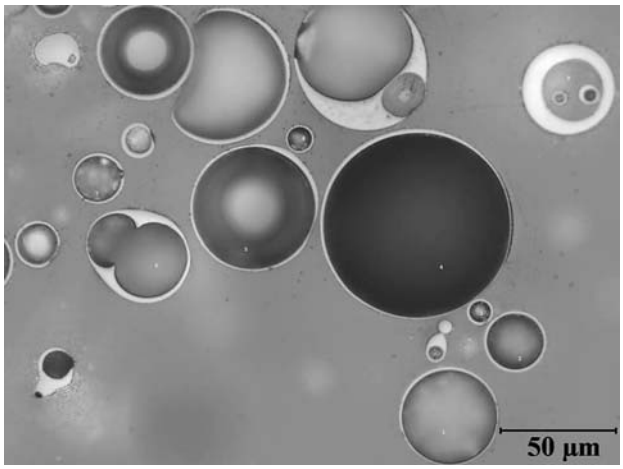

Figure 5 Polished cross-section of CMBs mounted in epoxy. This representative image of those used for quantitative microscopy also shows internal structure and variation in MB wall thickness.

be taken in the polishing procedure to minimize MB wall collapse and pull out during sample preparation. These images provide planar slices through MB mounted in epoxy, and thus any measurements made on the images do not necessarily reflect the actual diameter of the MB. Only those sections where an MB has been cut along its great circle provide accurate measurements of MB wall thickness and diameter. Fig. 6 illustrates this point. Fortunately, taking measurements of a 3-D structure on a 2-D image has been encountered frequently in stereology, so solutions are readily available. In order to obtain correct values we must calculate, statistically, values of diameter and wall thickness from the mean lineal intercept data measured on each image. Specifically, to correct diameter

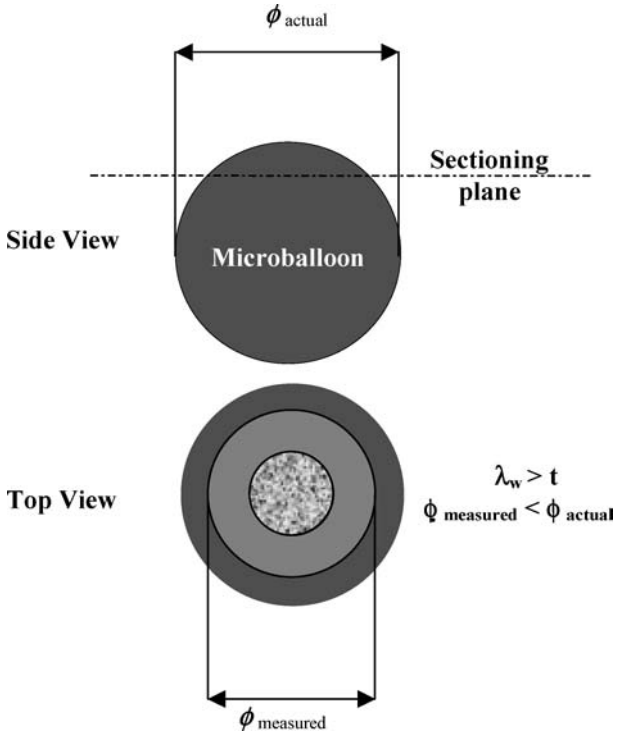

Figure 6 Schematic of MB sectioned above its great circle. Light grey region represents the sectioned surface, with diameter and thickness on the sectioning plane inaccurate as shown.

(ϕ) and wall thickness (t), the formulas are

$$\phi = \left(\frac{3}{4}\right)\lambda_{diameter} \tag{1}$$

$$\lambda_{wall} = \frac{4t(t^2 - 1.5t\phi + 0.75\phi^2)}{3(t^2 - t\phi + 0.5\phi^2)} \tag{2}$$

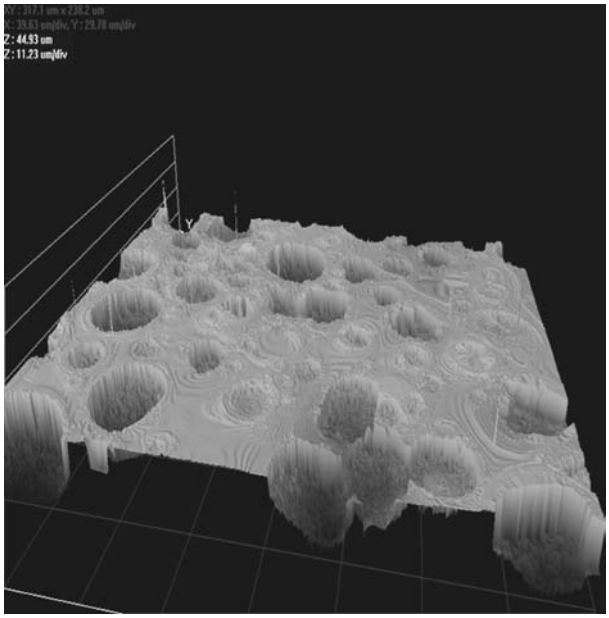

Figure 7 Optical interferometry image of 0.143 g/cm^3 tap density CMBs mounted in epoxy, allows direct measurement of wall thickness.

where λ is a measurement of thickness or diameter taken from mean lineal intercepts with the object of interest on the image [8, 9].

Both laser confocal and interference fringe analysis optical techniques yield similar 3D images of a polished microstructure. An optical microscope is used to image the sample surface, and computer software constructs a true 3D image of the sample surface. In the interferometry based system, the interference fringe patterns are analyzed and a 3D structure is calculated based on the analysis, whereas the laser confocal microscope uses monochromatic laser illumination and calculates where the in-focus portion of the image will be as the sample stage is moved vertically through focus. A movable aperture is used by the computer system to select only the focused area, and a stack of several focused 2-D images is formed such that the final 3D image is constructed by merging them along the vertical axis. Both systems yield similar results, as seen in Figs. 7 and 8. Both figures are 3D topologies of the sample shown in Fig. 5, and could easily be used to measure MB diameters and wall thicknesses.

A final optical microscopy technique, again interferometry-based, can be used to extract size measurements from MBs. This technique is applicable only to transparent MBs, such as GMBs and some PMBs. A dual-mirror interference microscope is used to image a single MB that is placed on one of the mirrors. The mirrors are then set so as to be slightly non-parallel. This yields an interference fringe pattern of light and dark concentric circles visible on the mirror. The focus is then adjusted until the darkest fringe is positioned on the MB, and the light source is switched from white to monochromatic. Fig. 9 demonstrates the correct setup. Then, one simply counts the number of reference fringes between the darkest fringe outside the MB and the MB itself. The wall thickness (t) of the MB can be calculated from the number of fringes (x), the wavelength of the monochromatic light source (λ), and the refractive index of the material (n') by using the following expression,

$$t = \frac{x\lambda}{4\,(n' - 1)} \tag{3}$$

This method has been shown to be accurate to within 0.05 μm for measuring GMB wall thickness [10].

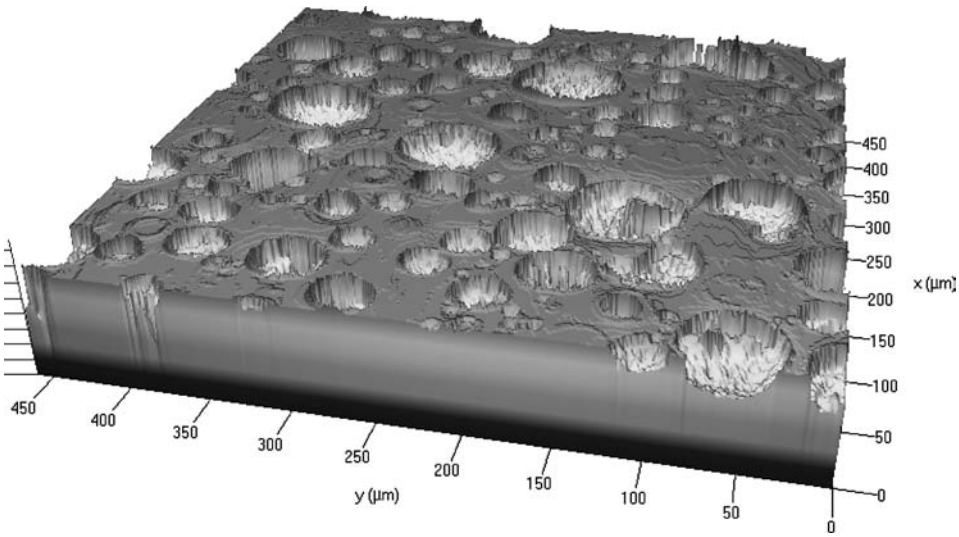

Figure 8 Laser confocal microscope image of 0.143 g/cm^3 tap density CMBs mounted in epoxy. Wall thicknesses standing proud with respect to the mount resin.

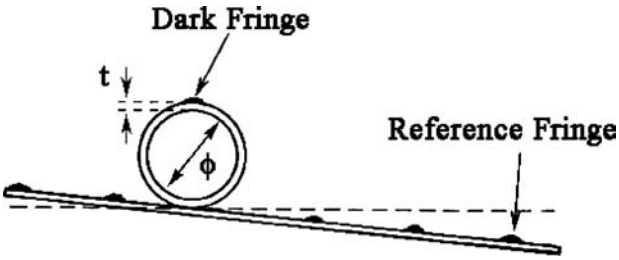

Figure 9 Schematic of interference light microscope configuration use to measure wall thickness of transparent MBs. After ref. [10].

3. Density of microballoons

Often, the density of MBs is of interest in determining other mechanical properties or can be used to distinguish between grades of MBs. Two separate methods are often used. One is pycnometry, where the volume occupied by a known mass of microballoons is measured by the volume of gas the MBs displace in a pressure chamber. Then, the balloon density is simply mass divided by volume. The other method uses ASTM Standard B 527, originally designed to measure the average settled density of metal or ceramic powder, to measure the average settled density of a manufacturing lot of MBs. To perform this test, 50 $\pm$ 0.2 g of MBs are placed in a 100 ml graduated cylinder, and then tapped 3000 times. The tap density of the MBs is their measured mass divided by the volume to which they settled after the vibration treatment. A schematic of this test is shown in Fig. 10 [11].

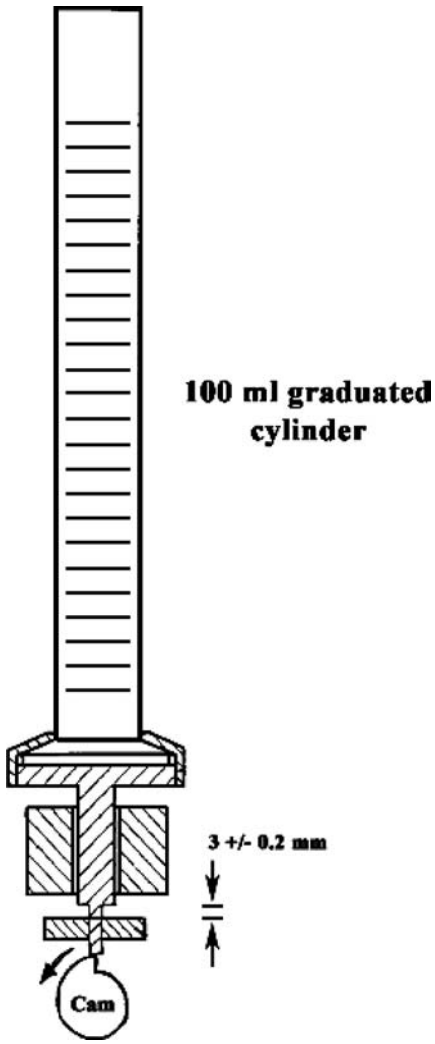

Figure 10 Schematic of tap density test apparatus for ASTM B 527. After ref. [11].

4. Compression test methods

4.1. Nanocompression of individual microballoons

Perhaps the most recent development in MB testing has been that of the compression of individual MBs. This has been possible by adapting a nanoindenter to function as a compression test frame, replacing the Berkovich tip with a flat-ended punch-like tip, and placing a flat, polished stub into the sample stage to function as a lower compression platen. The flat-ended punch is usually a sapphire cylinder with a flat tip of 90 μm diameter, but, recently a smaller square cross-sectioned diamond tip of 25 μm side length has proven successful. A schematic of this arrangement can be seen in Fig. 11. These compression tests give very accurate measures of failure load and indenter tip displacement.

Many different types of MBs have been tested via this technique, including CMBs, GMBs, uncured phenolic MBs, and cured phenolic MBs. Fig. 12 shows the different types of load-displacement behavior exhibited by these materials. As expected, MBs of traditionally brittle materials have well defined, mostly linear curves, whereas phenolic MBs display more ductility. The uncured phenolic does not even display a fracture point, but instead plastically deforms until totally flattened on

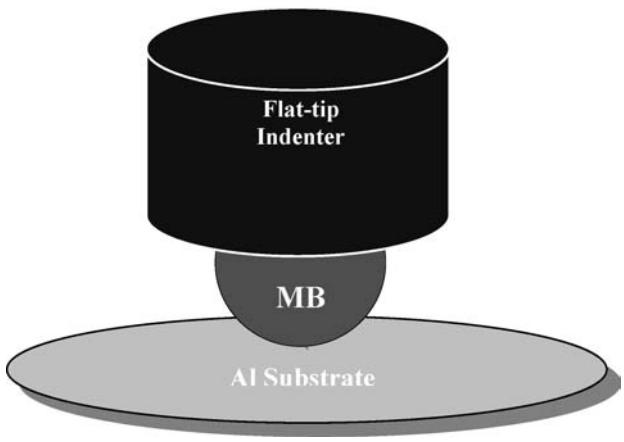

Figure 11 Schematic of nanoindenter modified for use in compression testing of MBs. After refs. [7, 8].

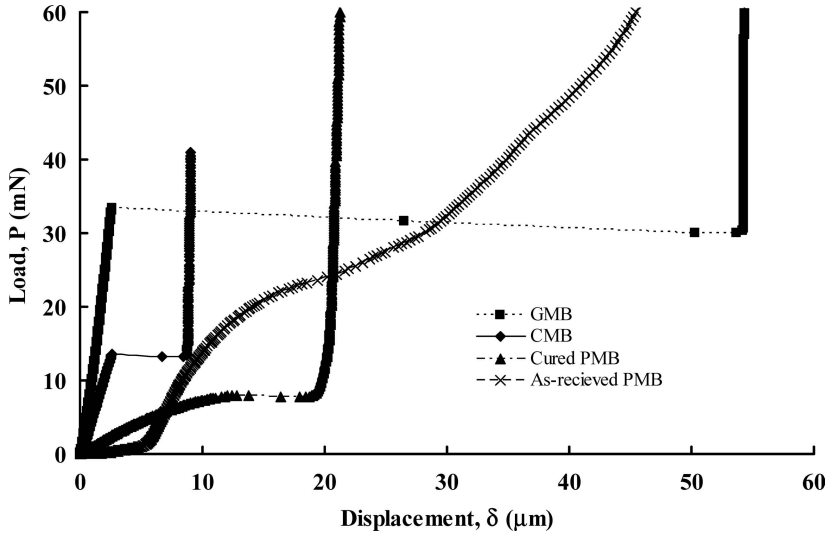

Figure 12 Compression curves from MBs composed of different materials. Note the brittle vs. ductile behavior.

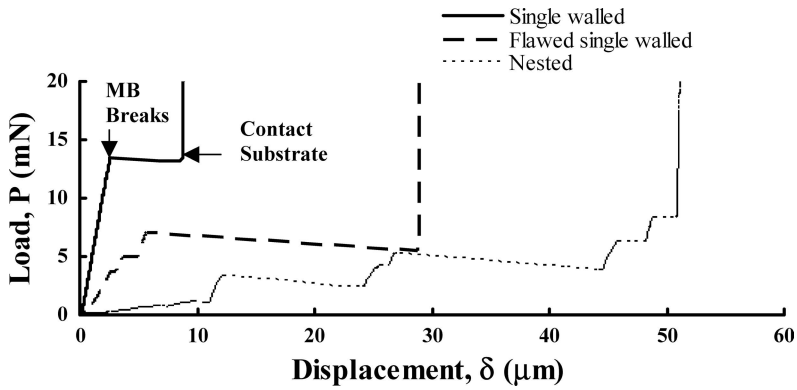

Figure 13 Possible types of compression behavior for brittle CMBs. After refs. [7, 8].

the substrate. This ductile vs. brittle behavior is not the only characteristic observable in load-displacement data. Morphological differences in microballoons may also be inferred from the shape of the curves. Fig. 13 provides an example, wherein we see three types of behavior from CMBs that can be related to their morphology. Single-walled microballoons possess one of the first two types of loading curves, whereas balloons with several internal compartments possess the confusing behavior is labeled nested in the figure. Figs. 2, 3, and 6 provide visual proof of the existence of such MBs in both glass and carbon. The flawed single-walled category of MB behavior was hypothesized to result from single walled microballoons that have holes or other imperfections in their walls.

Compression data provide several useful engineering parameters. Load (P_f) and displacement (δ_f) at failure are obtained directly from most load-displacement curves, the slope of the loading segment provides a pseudo-stiffness (k), and the work of fracture (W_f), defined as the area under the loading portion (or portions, for nested MBs) of the curve. The diameter of the MB in the loading direction, or vertical diameter (ϕ_v), is merely the difference in the displacement at initial loading and that when the indenter impinges upon the substrate. The compressive failure strain (ε_f) is calculated as the quotient of the displacement at failure and the vertical diameter, thus:

$$\varepsilon_f = \frac{\delta_f}{\phi_v} \tag{4}$$

These parameters provide a fairly wide range of property data, and average properties may of course be calculated for each type of MB. Additionally, trends between various parameters have been observed. For glass microballoons, which appear to be the most uniform type of MB under microscopic inspection, the authors have observed the trends shown in Figs. 14 and 15, relating failure load and work of fracture to diameter. Other types of microballoons examined by this technique have not shown these correlations, but tend to possess other, weaker correlations, due to their more irregular natures [7 , 8, 12].

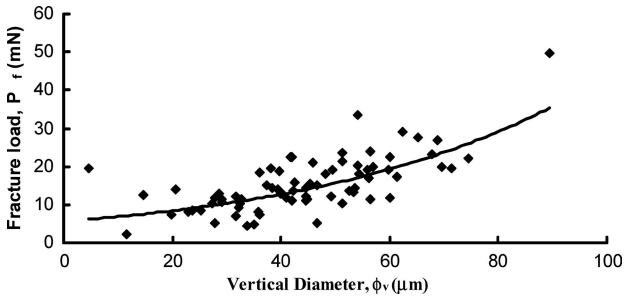

Figure 14 Direct correlation of failure load to MB diameter for GMBs (3M A16/500). After ref. [12].

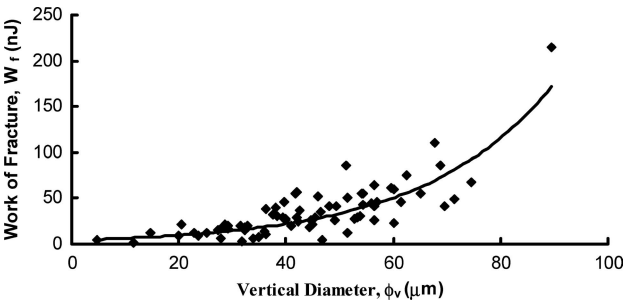

Figure 15 Work of fracture correlated favorably with MB diameter for GMBs (3 M A16/500). After ref. [12].

4.2. Microcompression of individual microballoons

This test technique, from Bratt *et al.* [13], utilized a custom developed compression apparatus to perform uniaxial compression on glass microballoons. The aim was to characterize the compressive strength of GMBs, especially focusing on testing that would relate to the durability of the MBs during mixing into polymer matrix composites. The test apparatus consisted of a motorized *x-y* stage, a stationary platen, and a conical flat-tipped rod to which an LVDT was attached. The MB was crushed between the platen and rod tip in essentially uniaxial compression, save for the affixing of the MB to the rod with epoxy. A force-time plot in compression was obtained for each MB, which was combined with a very precise measure of the wall thickness and diameter of each MB to yield stress-strain curves as explained below. These curves are generated based on an assumed failure at each MBs equator due to tensile stress. With this assumption, the stress and strain may be extracted from a "flexure test" model, giving stress at the MB's surface as

$$\sigma = \frac{F}{2\pi t^2} \tag{5}$$

and strain as

$$\varepsilon = \frac{54et}{d^2} \tag{6}$$

In Equations 5 and 6, F is the applied uniaxial compressive force, d is the MB diameter, and t is the wall thickness. Once stress and strain are known, Young's Modulus of the glass wall material was calculated from Hooke's Law. One overall trend was the clear dependence of failure load upon wall thickness, as seen in Fig. 16. Note that the trend line shown corresponds to an average failure strength (σ) of 2.2 GPa, which compares favorably to the well-documented tensile strengths of glass fibers [13].

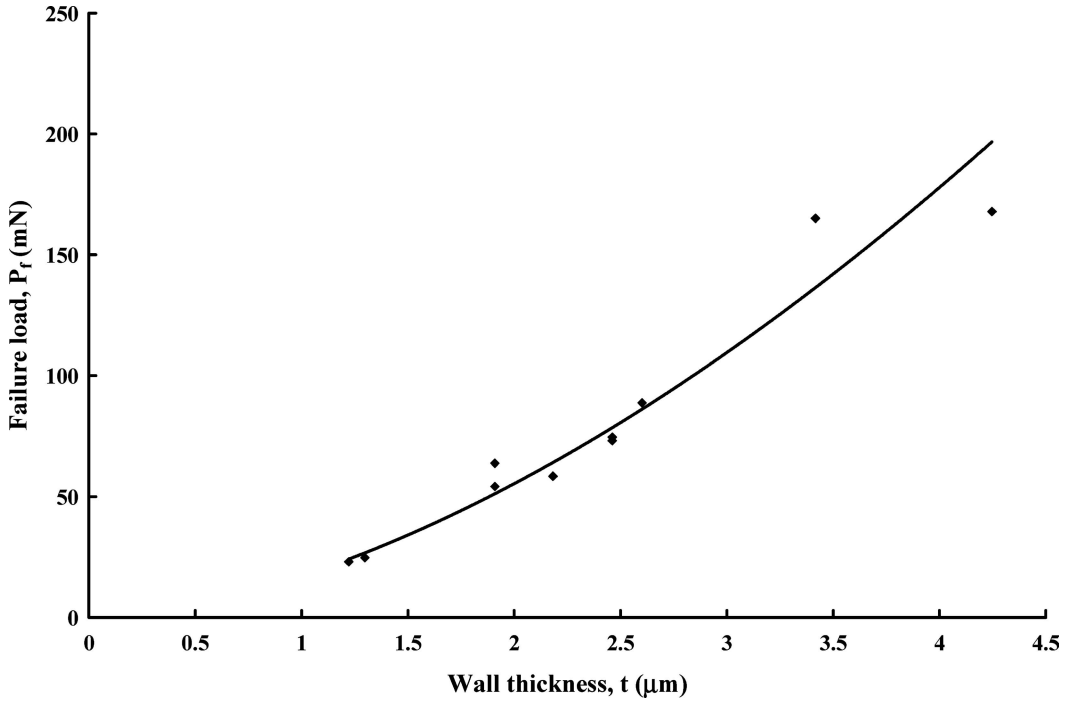

Figure 16 Failure load vs. measured wall thickness for GMBs, showing $P_f \alpha t^2$. After ref. [13].

4.3. Compression of individual macroballoons

Alumina hollow spheres of 1–5 mm diameters and 25–200 μm wall thickness were tested in uniaxial compression using a traditional mechanical test frame [14]. Raw data for this test was the failure load (F_c) of each hollow macroballoon. Unique to the Chung *et al.* [14] analysis is their definition of macroballoon strength (σ_s) as the quotient of the failure load of the macroballoon and its projected area, thus

$$\sigma_s = \frac{F_c}{0.25\pi d^2} \tag{7}$$

Equation 7 might appear to make an unprecedented use of the area of the macroballoons' great circle to normalize the raw loading data. This is not totally without justification, however. In the oil industry, small hollow particles were considered as proppants—small particles that will hold fissures in rock formations open—in petroleum wells. The strength of these proppants was successfully modeled in terms of a number of diametral contacts between close-packed hollow spheres that transfer a given force along each contact. When only a single contact is considered, the strength reduces exactly to that employed by Chung *et al*. Failure behavior of these macroballoons was also predicted via finite element modeling, and both experimental and modeling results confirmed failure primarily along horizontal or vertical diameters. Relative density of the macroballoons, as relating to solid Al_2O_3, was found to correlate with macroballoon strength, as Fig. 17 shows for both the experiments and the modeling. It can be seen that model overestimated the slope of the curve substantially; this discrepancy was attributed to "imperfections such as non-uniform wall thickness, imperfect sphere geometry, flaws, small tails, etc. [14]."

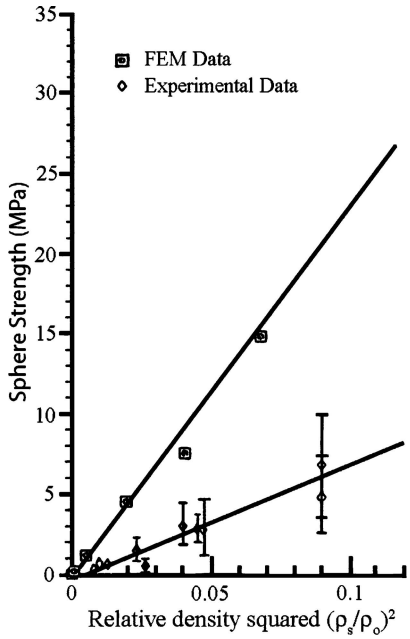

Figure 17 Strength vs. relative density squared for Al_2O_3 macroballoons. Linear relationships for both predicted and theoretical curves. After ref. [14].

4.4. Bulk isostatic compression of microballoons

This test method for microballoon characterization stems from the industrial need to characterize production lots of microballoons according to their compressive properties in a more efficient manner than individual compression provides. At one time, the procedure was an ASTM Standard, bearing designation D 3102-78, but it was withdrawn, for unknown reasons, in May 1984. Despite its withdrawal, it is still in use today as often the only test performed by MB manufacturers to characterize the compressive strength of their MBs. 3 M, for example, performs a slightly modified form of this test (3M QCM 14.1.5) on all of their GMBs except the highest strength grade, which is tested via the original ASTM method.

The basic premise of the test is to expose a batch of MBs to a high isostatic pressure, during which some of the MBs will collapse. The percent of MBs that collapse (or survive) is measured, and the MBs are classified according to the isostatic pressure at which a given percent of the MBs tested collapse (or survive). Both test methods place the MBs in a rubber container filler with either glycerin or isopropyl alcohol inside a pressure chamber. The ASTM test used oil as the working fluid, whereas the 3 M test employs nitrogen gas. Once the MB sample is in the pressure chamber, it is pressurized to a predetermined pressure while recording both pressure and volume. This process is repeated to get a second set of pressure-volume data, and both data sets are plotted as pressure vs. volume curves. The initial pressurization is known as the collapse curve, and the second pressurization provides the system compression curve. Fig. 18 provides an example of the two curves, which are used to determine the percentage of collapsed MBs in the test. Since air comparison pycnometry and a scale were used to determine the volume and mass of both the MBs and their rubber container prior to isostatic pressurization, the density of the MB wall material (ρ) can be used to find the volume of wall material (V_m) using the MB mass (M).

$$V_m = \frac{M}{\rho} \tag{8}$$

Next, the original volume (V_v) of the MB's interior void space is found by subtracting the volume of the wall material from the volume occupied by the MBs (V_{ap}), which is determined via the pycnometer.

$$V_v = V_{ap} - V_m \tag{9}$$

In Fig. 18, V_t refers to the total volume collapse, and is the difference in the collapse and compression curve values at

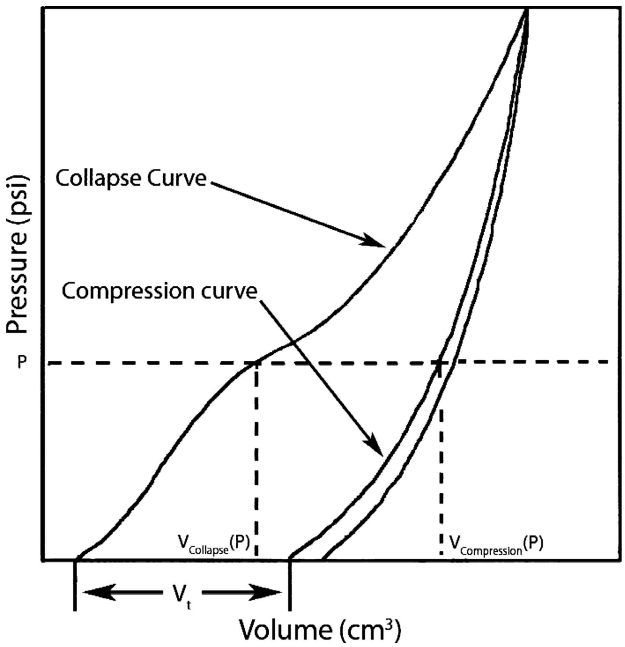

Figure 18 Compression curve from isostatic testing of batches of MBs, as per ASTM D 3102. % Survivors found from difference in compression and collapse curves. After ref. [6].

zero pressure. To calculate the fraction of collapsed MBs at a certain pressure level, the void volume collapsed at that pressure (V_p) is found as

$$V_p = V_t - (V_{compression}(P) - V_{collapse}(P)) \tag{10}$$

where $V_{Compression}(P)$ and $V_{Collapse}(P)$ are the volume values of the compression and collapse curves at the pressure of interest. Then, the percent volume collapse ($V_{Collapse}$) is found as

$$V_{collapse} = 100\left(\frac{V_p}{V_v}\right) \tag{11}$$

According to the ASTM standard, this percent void collapse was the only reportable parameter from isostatic testing; however, since the demise of the standard, the percent surviving MBs is often reported instead [6].

4.5. Isostatic compression of individual microballoons

Another variation of the isostatic pressure testing for MBs is to test each MB individually. This is not a variation of the ASTM test, in that it places a single MB into a special holder, which is located inside a pressure chamber with a quartz window. A stereomicroscope is used to image the MB in the chamber as pressure is applied. When visual observation indicates that the MB has collapsed, the chamber pressure is recorded and testing ceases. Bratt *et al.* [13] used the equations for the accepted failure mechanism, i.e., shell wall buckling, for a spherical pressure vessel

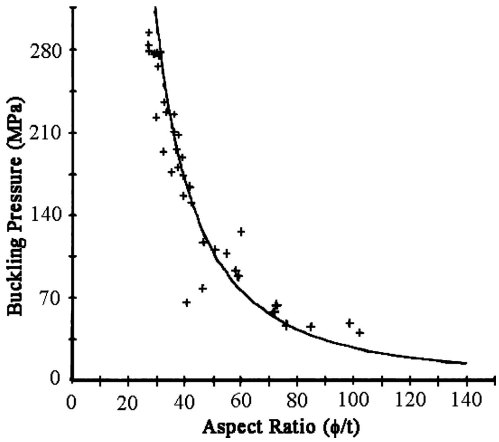

Figure 19 Aspect ratio vs. isostatic buckling pressure for individual GMBs. After ref. [13].

subjected to external isostatic pressure to predict a failure stress ($\sigma_{Failure}$) for MBs tested in this fashion as

$$\sigma_{Failure} = \frac{2E}{\left(\frac{\phi}{t}\right)\sqrt{3(1-\upsilon^2)}} \tag{12}$$

where E is the Young's Modulus and ν the Poisson's ratio of the MB wall material. Fig. 19 provides the results of this test for several GMBs, where the trend line was calculated using a Young's Modulus of 56.5 GPa and a Poisson's ratio of 0.21. Note the agreement between the calculated curve and the experimental data points [13].

5. Tensile test methods

5.1. Mechanical tensile testing

Surprisingly, MBs have been successfully tested in tension, although the test doubtlessly was not purely tensile loading. The test technique, developed and employed solely at Los Alamos National Labs in the late 1970s, involves bonding two small brass rods to opposite ends of a GMB's diameter. Care is taken during bonding to ensure that a small region between the rods was left free of epoxy, providing the gage length. These rods provide the grip regions for the ensuing tensile pulling of the MB in a loading frame designed specially for the test. The loading apparatus consisted of a dynamometer (mounted on a xyz translation table), from which load at failure was recorded. This test method appears to have been the only one of its kind, and was only used on a few specific batches of KMS and 3 M microballoons [15].

5.2. Tensile burst testing

This method was also conceived and executed solely at Los Alamos National Labs during the late 1970s for quality verification of KMS and 3 M GMBs. It is performed

by sealing a single GMB inside a quartz tube and heating to 350°C while pressurizing the tube with helium. The critical step here is the pressurization rate, which must be carefully increased to avoid bursting of the MB by external pressure, allow sufficient time for the helium to diffuse through the MB walls, and allow pressure equalization between the interior and exterior of the MB. According to Milewski and Marsters [15], for a 1 μm wall thickness GMB of 500 μm diameter, a final pressure of 2.07 MPa can be reached at 30.23 MPa/min, and must be held for 10 min to achieve equilibrium conditions. Then, the temperature is decreased to room temperature, and the pressure in the quartz tube is decreased until the MB bursts due to internal pressure. The MB is observed throughout the experiment via a stereomicroscope, and upon failure, the pressure difference supported by the MB walls is recorded. The pressure differential can be used to calculate the maximum tensile stress in the MBs wall according to

$$\sigma = \frac{\Delta P \phi}{4t} \tag{13}$$

Equation 13 is in terms of the tensile stress (σ), the pressure differential at failure (ΔP), the MB's diameter (ϕ), and the wall thickness (t) of the MB. The results of this test were compared to the uniaxial tensile testing technique and were observed to yield similar but lower values. These lower values were expected, due to the greater probability of stressing a critical flaw when subjecting the entire MB to loading, rather than just a particular gage length [15].

6. Nanoindentation

Nanoindentation has become a routine method for determining the modulus and hardness of a material or of a phase therein, but, until recently, had not been applied to MBs. The method for indenting MBs successfully involved a single key step—the mounting and polishing of MBs in epoxy resin. Fig. 5 provided an example of such a cross-section. Several samples such as this were indented in an MTS Nanoindenter XP II, and the continuous stiffness measurement technique was used to determine the hardness and Young's Modulus from indents located in the thick regions of the carbon walls. Data from these tests must only be taken from relatively shallow indentation depths, as the wall beneath the surface curves, and therefore limits the volume of material available for indentation. The necessity of 500 nm or less indentation depths placed instrument calibration and tip sharpness as critical parameters that were carefully checked before each test batch. The white arrow in Fig. 20 shows the location of a successful indentation on a 0.143 g/cm^3 tap density CMB, and Fig. 21 provides the corresponding Young's modulus vs. displacement into surface curve for this point. Overall, this technique has provided the only measure of Young's Modulus for these CMBs (average was 12.76 GPa), and could easily be adapted to any type of MB that could be mounted in epoxy and polished.

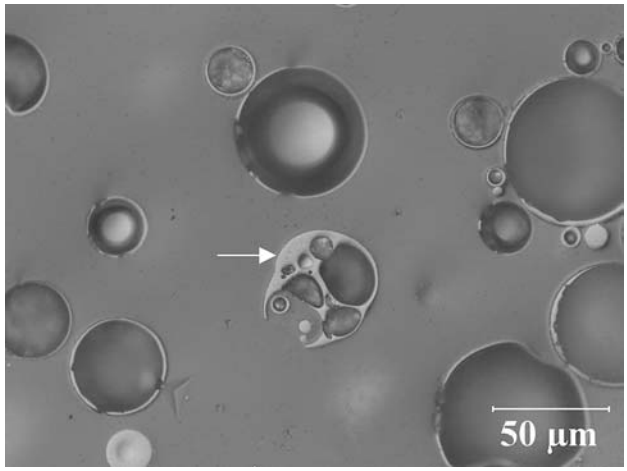

Figure 20 Optical image of 0.143 g/ml tap density CMBs used for nanoindentation. Indent located in CMB wall at white arrow. Fiducial indents also visible at lower left.

7. Synergy of test techniques

Obviously, thorough characterization of the morphology and properties of microballoons requires a combination of the above techniques to obtain structure–property relationships. Information on morphology requires some sort of microscopic examination, but there are advantages and disadvantages to most methods. If the MBs to be examined are transparent, then the interference technique described by Weinstein [10] will yield the best measure of wall thickness and diameter; however, for opaque MBs, the best method depends on what type of information is needed. SEM is a direct measurement method, but suffers if large amounts of data must be gathered, i.e., a wide variation in wall thicknesses exists in the study population or a small confidence interval is desired. Conventional optical microscopy coupled with statistically valid stereological formulas is best suited to analyzing massive data volumes, but then calculation accuracy in statistical correction becomes an issue. The interference fringe analysis and laser confocal techniques both would seem to alleviate this difficulty with optical imaging, since direct measurements of diameter and thickness are possible.

Characterization of MB mechanical properties also requires a combination of testing techniques, depending upon what mechanical property is relevant. To predict the MBs load-bearing ability in conventional syntactic foams, isostatic pressure testing provides a reasonable measure of the balloons' survivability under various loading, as is also true with their ability to be injection molded. Of

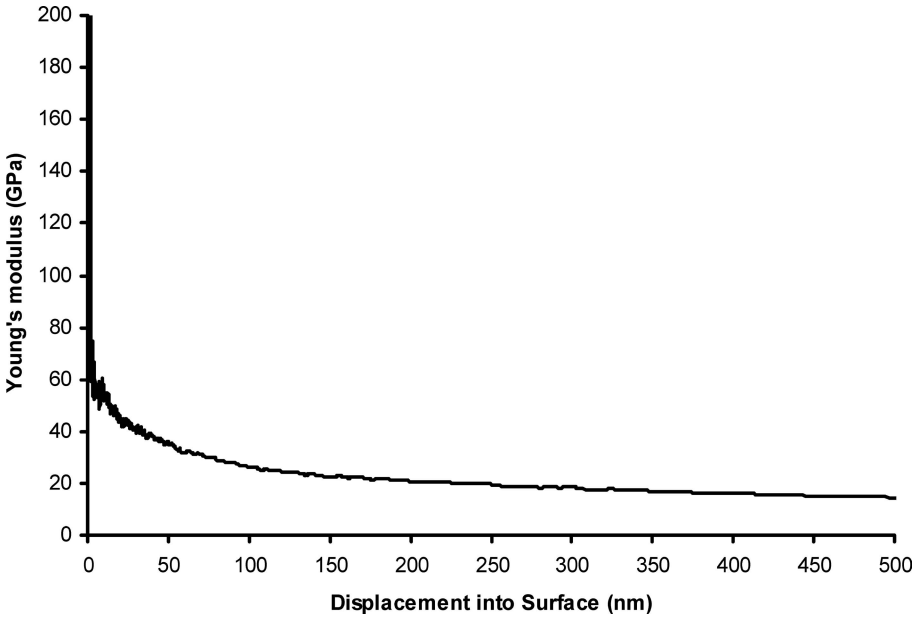

Figure 21 Modulus vs. displacement curve for indent in Fig. 20. Average modulus between 100 and 500 nm was 20.409 GPa.

the two isostatic test methods, the bulk test is clearly faster and more applicable to industry. Uniaxial compression data from microballoons is thought to relate more to the MBs durability in handling and mixing with polymers for syntactic foam construction. Of the methods for MB compression, none would scale well for commercial use, although the nanoindenter compression technique has been used for initial product evaluation and comparison between small populations with different processing parameters. The additional benefit here is the growing availability and reliability of nanoindentation equipment; not only can compressive properties be obtained, but the same instrument is also the only one that can provide Young's modulus of MBs. Of course, these techniques need simultaneous application of microscopic examination to extract both wall thickness and diameter from the MBs to realize maximum utility. In the realm of tensile testing of MBs, neither method has seen significant use outside a laboratory setting. While the burst test could provide useful data to complement isostatic crushing of single MBs, the uniaxial tensile procedure does not necessarily test the MB in pure tension, and may therefore not be of much value. So, the choice of method for mechanical property assessment should consider the anticipated stress states likely to be encountered in specific applications.

Further, evaluation of actual and potential reactions of MB, and foams in which they are incorporated, can be aided by 2-D and 3-D modeling. Commercially available software packages, as well as application specific programs, require input values from many of the techniques described. Both idealized and actual microstructures and MB morphologies can be hypothesized and evaluated for given applications.

8. Conclusions

By combining electron and optical microscopic techniques with novel mechanical testing, microballoons may be characterized in terms of both their morphology and mechanical properties. Microballoon wall thickness, diameter, and sphericity are all determinable by microscopy, and these results aid in the analysis of the compressive loading data from various test procedures. Isostatic compression of both individual and bulk microballoon samples can be used to determine failure strengths, uniaxial compression tests are available for failure load determination, and some tensile testing has been performed. Additionally, nanoindentation of microballoon wall materials has been proven to be a method for obtaining hardness and modulus. Together, all of these techniques can provide both manufacturers and customers a better understanding of microballoons' performance.

Acknowledgements

Partial support for this work was provided by Los Alamos National Laboratory/DOE subcontract #44277-SOL—02 4X. K. B. Carlisle is grateful to the Department of Defense for a National Defense Science and Engineering Graduate Fellowship.

References

1. H. L. PRICE and J. B. NELSON, *J. Comp. Mater.* **10** (1976) 314.
2. F. VEATCH, LYNDHURST, and R. W. BURBANS, *Process of Producing Hollow Particles and Resulting Product*. 1953, The Standard Oil Company: United States.
3. K. ESUMI, S. ESHIMA, Y. MURAKAMI, H. HONDA and H. ODA, *Colloids and Surfaces A: Physicochemical and Engineering Aspects* **108**(1) (1996) 113.
4. A. BOURLINOS, N. BOUKOS and D. PETRIDIS, *Adv. Mater* **14**(1) (2001).

5. W. R. BECK and D. L. O'BRIEN, Glass Bubbles Prepared by Reheating Solid Glass Particles. (Minnesota Mining and Manufacture Co., USA, 1963) p. 5.
6. *ASTM D 3102-78: Standard Practice for the Determination of Isostatic Collapse Strength of Hollow Glass Microspheres*. American Society for Testing and Materials. (1984).
7. G. GOUADEC, K. CARLISLE, K. K. CHAWLA, M. C. KOOPMAN, G. M. GLADYSZ and M. LEWIS, Nano-compression of carbon micro-balloons with a flat-ended cylindrical indenter. in Indentation Techniques in Ceramic Materials Characterization, Apr 27-30 2004 (American Ceramic Society, Nashville, TN, United States, 2004).
8. K. CARLISLE, K. K. CHAWLA, G. GOUADEC, M. KOOPMAN and G. M. GLADYSZ, Nanocompressive properties of carbon microballoons and mechanical properties of carbon based syntactic foam composites. in ICCM-14. (Society of Manufacturing Engineers, San Diego, CA 2003).
9. R. T. DEHOFF and F. N. RHINES (Eds.), in "Quantitative Microscopy" (McGraw-Hill, New York, 1968).
10. B. W. WEINSTEIN, *J. Appl. Phys.*, **46**(12) (1975) 5305.
11. ASTM B 527: Standard Test Method for Determination of Tap Density of Metallic Powders and Compounds (American Society for Testing and Materials, 2000).
12. M. KOOPMAN, G. GOUADEC, K. CARLISLE, K. K. CHAWLA and G. GLADYSZ, *Scripta Materialia* **50** (2004) 593.
13. P. W. BRATT, J. P. CUNNION and B. D. SPIVAK, in Mechanical Testing of Glass Hollow Microspheres, in Advances in Materials Characterization, edited by D. R. Rossington, R. A. Condrate and R. L. Snyder, (Plenum Press, New York, 1983) p. 441.
14. J. H. CHUNG, JOE K. COCHRAN and KON J. LEE, *Mat. Res. Soc. Symp. Proc.* **372** (1995) 179.
15. J. V. MILEWSKI and R. G. MARSTERS, *J. Vac. Sci. Technology* **18**(3) (1981) 1279.